UFMTrack: Under-Flow Migration Tracker enabling analysis of the entire multi-step immune cell extravasation cascade across the blood-brain barrier in microfluidic devices

Mykhailo Vladymyrov[1,2], Luca Marchetti[1], Sidar Aydin[1,+], Sasha Soldati[1], Adrien Mossu[1], Arindam Pal[1,Δ], Laurent Gueissaz[1,◊], Akitaka Ariga[3,□], and Britta Engelhardt[1]

[1] Theodor Kocher Institute, [2] Data Science Lab, and [3]Laboratory for High Energy Physics, University of Bern, Bern, Switzerland

present address: [+] Department of Pharmacology, University of California, San Diego; [Δ] Department of Biomedical Engineering, University of Texas at Dallas; [◊]Department of Neuroscience, Karolinska Institutet, Stockholm, Sweden; [□] Laboratory for Elementary Particle Physics, Department of Physics, Chiba University, Chiba, Japan

Correspondence:

Dr. Mykhailo Vladymyrov

Theodor Kocher Institute

University of Bern, Bern, Switzerland

mykhailo.vladymyrov@tki.unibe.ch

Authors contribution

M.V. implemented the UFMTrack software framework, carried out automated analysis and performance evaluation, and contributed to experimental design and imaging.

M.V. and B.E., wrote the manuscript with contribution form S.S., S.A. and L.M.

M.V. with contribution from S.A., L.M. and S.S. conceptualized the T-cell migration analysis pipeline.

L.M., S.A. and S.S. Carried out the experiments and imaging.

S.A., L.M., A.M., and M.V. performed annotation of the datasets for the segmentation model training.

S.A., L.G., A.P., and M.V. performed manual data analysis.

A.A. and B.E. designed the research together with M.V., acquired funding, and coordinated the collaboration.

Abstract

The endothelial blood-brain barrier (BBB) strictly controls immune cell trafficking into the central nervous system (CNS). In neuroinflammatory diseases such as multiple sclerosis, this tight control is however disturbed leading to immune cell infiltration into the CNS. The development of *in vitro* models of the BBB combined with microfluidic devices has advanced our understanding of the cellular and molecular mechanisms mediating the multi-step T-cell extravasation across the BBB. A major bottleneck of these *in vitro* studies is the absence of a robust and automated pipeline suitable for analyzing and quantifying the sequential interaction steps of different immune cell subsets with the BBB under physiological flow *in vitro*.

Here we present the Under-Flow Migration Tracker (UFMTrack) framework and a pipeline built with it to study the entire multi-step extravasation cascade of immune cells across brain microvascular endothelial cells under physiological flow *in vitro*. UFMTrack achieves 90% track reconstruction efficiency and allows for scaling due to the reduction of the analysis cost and by eliminating experimenter bias. This allowed for performing an in-depth analysis of all behavioral regimes involved in the multi-step immune cell extravasation cascade. The study summarizes how UFMTrack can be employed to delineate the interactions of $CD4^+$ and $CD8^+$ T cells with the BBB under physiological flow.

Author summary

Immune cells continuously travel through our body to perform immune surveillance. They travel within blood vessels at a very high speed, and slow down upon reaching their target organ by the sequential interaction with different adhesion and signaling molecules on the vascular endothelial cells.

The study of molecular mechanisms mediating this multi-step extravasation of immune cells has been significantly advanced by *in vitro* cultures of microvascular endothelial cell monolayers. The

dynamic interaction of the immune cells with endothelial monolayers can be imaged over time *in vitro* in microfluidic devices under physiological flow. The manual analysis of the acquired imaging data is time-consuming and prone to experimenter error. Analysis automation is however hampered by the similar appearance of the unlabeled immune and endothelial cells, and by the flow causing rapid immune cell displacement.

Here we introduce UFMTrack, the under-flow migration tracker framework allowing for automated analysis of immune cell interactions with microvascular endothelial cells under flow *in vitro*. UFMTrack performs comparably to manual analysis of an experienced researcher, eliminates experimenter's bias, and improves the accuracy of the immune cell tracking. Taken together, UFMTrack sets the stage for scalability of *in vitro* live cell imaging studies of immune cell extravasation.

Keywords

Automated analysis, blood-brain barrier, cell tracking under flow, deep learning, flow chamber, leukocyte trafficking, live cell imaging, machine learning, microfluidics, multiple sclerosis, T cell

Introduction

Immune cells continuously travel throughout our body as a means of immune surveillance. Moving within the bloodstream allows for their fast transport to even distant sites but requires extravasation once they have reached their target organ. Immune cell extravasation across the vascular wall is a multi-step process regulated by the sequential interaction of different signaling and adhesion molecules on the endothelium and the immune cells (1,2). These molecular interactions mediate distinct sequential steps, namely tethering and rolling to reduce travel speed, shear resistant arrest, polarization and crawling of the immune cell on the luminal surface of the endothelium, and finally immune cell diapedesis across the endothelial layer (1,3,4).

The precise molecular mechanisms mediating the multi-step immune cell extravasation in each organ depend on the immune cell subset but also the specific characteristics of the vascular bed. For example, in the central nervous system, the endothelial blood-brain barrier (BBB), establishes a tight barrier that strictly controls the transport of molecules across the BBB, ensuring tissue homeostasis required for neuronal function. The BBB similarly controls immune cell trafficking into the CNS. Thus, accounting for these special barrier properties, unique characteristics of the multi-step T-cell migration across the BBB have been described. For instance, T cells crawl for very long distances against the direction of blood flow on the surface of the BBB endothelium in search of permissive for diapedesis locations (5–7). Research on T-cell interaction with the BBB has been already successfully translated into therapies in the clinic (8,9).

Exploring the entire multi-step extravasation of immune cells across the BBB has been significantly advanced by making use of *in vitro* BBB models maintaining their barrier properties and placing them into microfluidic devices. Combined with microscopic setups that allow for *in vitro* live-cell imaging of the immune cell interaction with the brain endothelial monolayer under physiological flow over time, the molecular mechanisms mediating the sequential interaction of T cells during extravasation across the BBB have been delineated (1). These studies have shown that upon their

arrest, T cells polarize and either crawl at speeds between 3 to 10 µm/min over the brain endothelial monolayer or probe the endothelial monolayer by remaining rather stationary and sending cellular protrusions into the endothelial monolayer (10,11). Both processes can lead to diapedesis of the T cells across the brain endothelial monolayers, a process that lasts at least 3 to 5 minutes, with some immune cells observed to protrude and retract several times prior to finalizing a prolonged diapedesis process to the abluminal side of the brain endothelial monolayer (7,12). Finally, T cells that have successfully migrated across the brain endothelial monolayer usually continue to migrate underneath the endothelial monolayer (13,14).

The data analysis of these "*in vitro* flow assays" requires time-consuming offline frame-by-frame analysis of the imaging data by individual experimenters, in which the dynamic interactions of each individual immune cell has to be followed over the entire time of the assay manually and assigned to specific categories. Performing such analysis is tedious and an accurate assignment of the different T-cell behaviors requires experience. Thus, this manual analysis is prone to inevitable errors as well as to subjective judgments of the different experiments. Furthermore, the time-consuming manual T-cell tracking limits the number of events that can be studied and thus also the statistical power of the analysis.

Automation of the analysis of the recorded multi-step T-cell extravasation across the BBB in the microfluidic device would thus be highly desirable. It is however hampered as these assays are usually performed with unlabeled cells and imaged by phase contrast, which poses a challenge due to the similar grayscales and morphology of the immune cells interacting with the brain endothelial cells. Further challenges include superfused T cells that in the presence of shear flow instantly appear within the field of view (FoV) and are either suddenly displaced over a certain distance or completely detached and washed away. Proper analysis of these events is mandatory for reliable T-cell tracking but also with respect to the analysis of the overall avidity of the dynamic T-cell interaction steps with the underlying brain endothelium. Thus, it was compulsory to establish a

125 tracking solution that accounts for the effect of the flow on the migrating cells and the distinct
126 migration regimes.

127 Here we introduce the developed under-flow migration tracker (UFMTrack) framework that
128 systematically addresses the above-mentioned hurdles, allowing it to perform automated tracking
129 and analysis of cell-cell interactions. We also show a successful implementation of UFMTrack to
130 build an analysis pipeline for T-cell interactions with brain microvascular endothelial cells *in vitro*
131 under physiological flow. UFMTrack reaches 90% T-cell tracking efficiency, performing comparably to
132 manual analysis while eliminating the experimenter's bias and improving the accuracy of T-cell
133 tracking. Therefore, it enables significant savings in the labor force and time for data analysis.

134

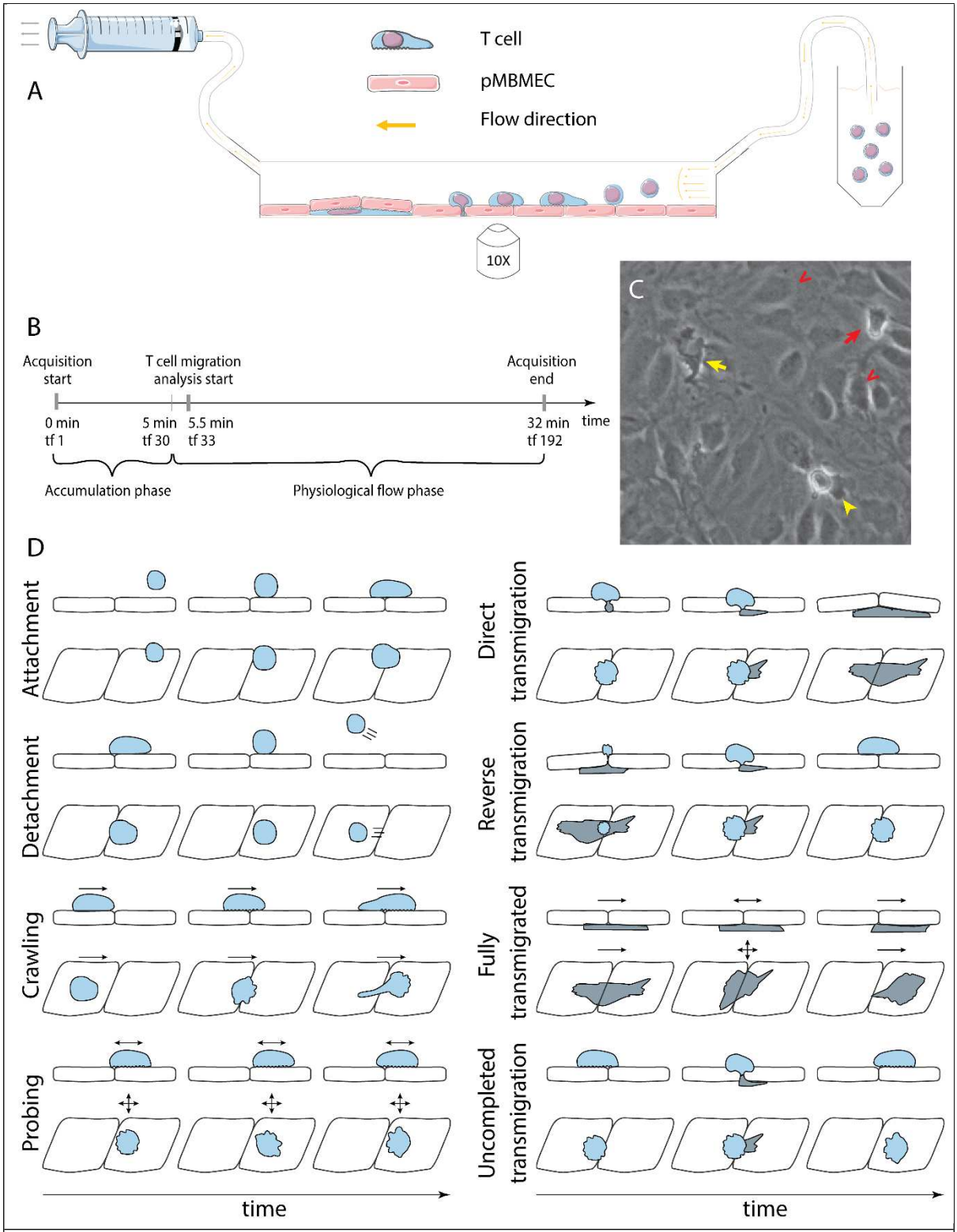

Figure 1. ***In vitro*** **analysis of the multistep cascade of T-cell migration across the BBB model under physiological flow. A.** *In vitro* under-flow assay setup. T cells were superfused on the pMBMEC monolayer and their migration under flow was observed using phase-contrast imaging modality. Imaging was performed with a time step of 10 sec/timeframe. **B.** *In vitro* flow assay timeline. During

the accumulation phase under flow with the shear stress of 0.1 dynes/cm^2 T cells adhered to the pMBMEC monolayer. After 5 min (timeframe 30) the shear stress was increased to 1.5 dynes/cm^2, leading to rapid detachment of not firmly adhering T cells. Analysis of the post-arrest T-cell behavior was thus starting at 5.5 min (timeframe 33). tf = timeframe. **C.** Example of phase-contrast imaging data. Red arrow – crawling T cell; yellow arrow – fully transmigrated T cell; yellow arrow-head – transmigrated part of a partially transmigrated T cell; red V arrowheads – pMBMECs. **D.** Schematic representation of distinct T-cell behavior regimes that are detected and analyzed using the developed UFMTrack framework. Crawling cells migrate continuously, while probing cells interact with the pMBMECs and move around the interaction point within 2 cell-size ($20\ \mu m$) as indicated by the arrows. Side and top views are shown.

Results

To design and develop the automated T-cell under-flow migration analysis framework UFMTrack framework presented here, we made use of *in vitro* imaging datasets following T-cell migration across primary mouse brain microvascular endothelial cells (pMBMECs) under physiological flow *in vitro*. The framework combines three components: T-cell segmentation and transmigration detection, T-cell tracking under flow, and analysis of each of the steps of the multistep T-cell migration cascade. Segmentation and transmigration detection of the T cells, migrating on the pMBMECs is performed with a 2D+T U-Net-like convolutional neural network (15). T-cell under-flow tracking algorithm was formulated as a constrained optimization problem.

Next, we describe the methods and algorithms employed to develop UFMTrack. Links to the code and the datasets used for model training can be found in the Data Availability section.

149 ***I. T-cell segmentation***

150 Reliable cell segmentation is crucial for reliable cell tracking. In the phase-contrast imaging
151 modality, it was impossible to achieve reliable differentiation between T cells and endothelial cells of
152 the pMBMEC monolayer based on pixel intensity. For detection of T-cell transmigration across
153 pMBMEC monolayers (diapedesis), sufficiently reliable cell segmentation of the transmigrated T cells
154 was also required. To achieve this, we have designed 2D and 2D+T U-Net like (15) fully convolutional
155 neural network-based models for multitask learning. The models were trained for the prediction of
156 three maps: cell probability, the probability that the T cell is below the pMBMEC monolayer, and cell
157 centroids. The models performed predictions based on the gray-scale of the respective phase-
158 contrast images in the case of the 2D model, or sequences of 5 timeframes in the case of the 2D+T
159 model. The models were implemented in TensorFlow (16). The training was performed using the
160 annotation mask for T cells ("T cell mask") and the mask of the transmigrated part of the T cells
161 ("transmigration mask"), the centroids map, and the weight map (Figure 2).They have approximately
162 3M and 8M parameters correspondingly and the model architectures are summarized in
163 Supplementary Tables 1, 2. Details on models' implementation, training and image processing can be
164 found in the "Segmentation models" section of the Supplementary Material.

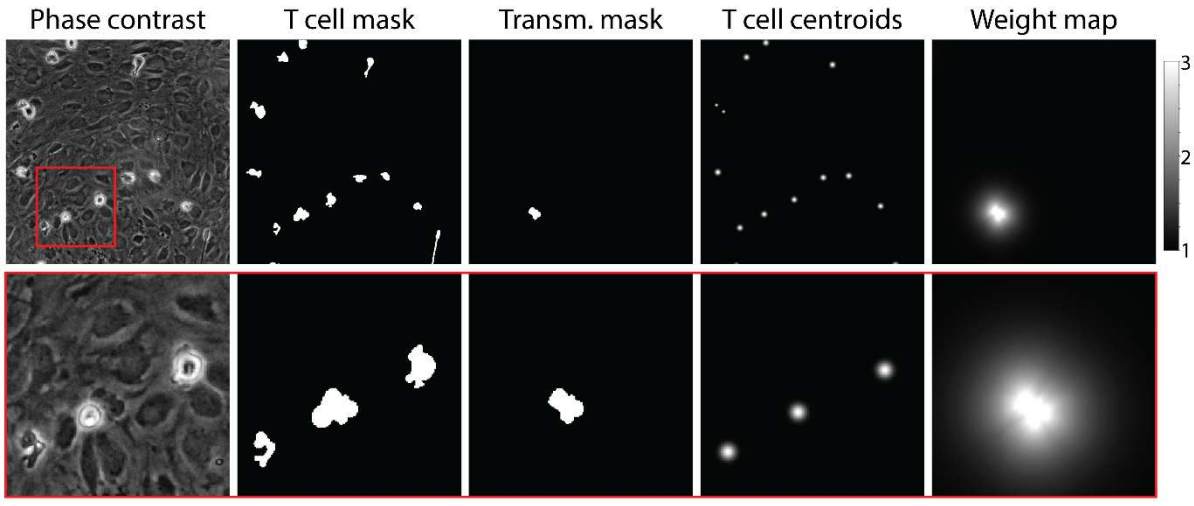

Figure 2. Example of data used for training of the T-cell segmentation model. From left to right: Phase-contrast microscopy image of T cells migrating on top of the pMBMEC monolayer;

annotated T cell mask; annotated mask of transmigrated part of T cells; T cell centroids; w_{cell} weight map. The bottom row shows zoom-in on the highlighted area.

For the prediction of the T cell mask the 2D+T model outperformed the 2D model by notable 9% according to the average precision (AP) metric (Table 1). At the same time for the transmigration mask, which is much more difficult to infer, the 2D model performance reached only 54% which is not sufficient for reliable detection of T cells that had migrated across the pMBMEC monolayer. In this task, the 2D+T model outperformed the 2D model by 32% AP. We observed that the 2D+T model was sensitive to frame misalignment, leading to false positive detection of transmigrated T cells. Thus, to generate the preliminary T-cell masks used for frame alignment and histogram normalization we employed the 2D model. Afterward, for the T-cell segmentation and transmigration detection, we employed the 2D+T model, followed by a watershed algorithm based on the inferred T cell mask and the cell centroids as seed points. A stitched phase-contrast image sequence can be seen in Supplementary Video 1, and overlayed with the segmented cells and highlighted transmigration mask in Supplementary Video 2.

Table 1. Comparison of the performance of the 2D and 2D+T-cell segmentation models.

	Performance, AP	
	2D	2D+T
T Cell mask	86.12%	95.26%
Transmigration mask	50.56%	82.74%

After segmentation we suppressed the noise by discarding small objects with an area below 30 pixels (mean area of a T cell is about 400 pixels). For each T cell we evaluated its coordinates as

geometric mean coordinate, angle of the longer axis, and elongation $\epsilon = \sqrt{\frac{\sum_i (x_i' - x_0')^2}{\sum_i (y_i - y_0')^2}}$, where x_i', y_i' are projections of the i-th T cell mask pixel coordinates on the orthogonal long and short axes of the T cell, and x_0', y_0' are the corresponding projections of the geometrical center of the T cell, and the summation is performed over all T cell mask. Additionally we evaluated the mean T cell probability $\overline{p_{cell}} = \frac{1}{n_{pix}} \sum_i p_{cell,\,i}$, mean transmigration probability $\overline{p_{tr}} = \frac{1}{n_{pix}} \sum_i p_{tr,\,i}$, and cell transmigration coefficient as $t_c = \frac{1}{n_{pix}} \sum_i \frac{\min(p_{tr,\,i}, p_{cell,\,i})}{p_{cell,\,i}}$, where n_{pix} is number if cell pixels and $p_{cell,\,i}$, $p_{tr,\,i}$ are the T cell and transmigration probabilities for i-th pixel in the predicted T cell mask.

II. T-cell tracking

The presence of flow causes several types of discontinuous events that were managed with a specialized tracking algorithm. These are: 1) the sudden appearance of T cells in the field of view (FoV), 2) the sudden detachment of a T cell followed by its disappearance from FoV, and 3) the displacement over larger distances of T cells that do not adhere firmly to the pMBMECs. The primary inspiration for our approach was the Conservation Tracking algorithm (17). By performing global optimization constrained to controlled probabilities of T-cell appearance, disappearance, and displacement due to the flow at every time point, we could consistently reconstruct the T cell tracks. This procedure favors the reconstruction of long T-cell tracks, while at the same time allowing for tracking of the T cells which detach or are displaced by the flow ("accelerated T-cell movement") over a longer distance ($> 8\ \mu m$) with speed significantly higher than their crawling speed.

The tracking consists of four main steps: linking, search for track candidates, global track consistency resolving, and resolving the track intersections. At the linking step we identified all possible connections of T cells between the timeframes (Figure 3C).

Next, during the search for track candidates step, we aimed to find continuous track segments of T cells or under-segmented groups of T cells crawling on top of or below the pMBMEC monolayer without accelerated movement segments on the T cell track characterized by rapid T cell displacements. The whole dataset of T cells across all time points was represented as a graph. Each vertex corresponds to a T cell (multiplicity m=1), or a group of potentially under-segmented T cells (m>1). The vertices are connected according to links obtained at the linking step. Track segments were found by performing global optimization to find consistent connectivity of vertices across the time points (Figure 3D), by employing an approach inspired by the conservation tracking algorithm summarized in Schiegg et al. (17). Optimization was performed using the CP-SAT constrained optimization procedure using the open source OR-Tools library (18).

Next, resolving global track consistency was performed. In this step, the scope of T cell tracking is shifted from individual nodes (representing T cells at individual timeframes as well as groups of under-segmented T cells) to the track segments – unambiguous sequences of nodes, and vertices at the endpoints of the segments. These are track start and end points, points of merging and separation of track segments in case of under-segmentation, as well as ambiguous points on a track. The latter was identified by sudden T cell displacement, which is a hallmark of detaching and reattaching T cells and T cells transitioning from properly segmented to under-segmented T cells or vice versa (Figure 3E). This was followed by the search for potential missing track segments due to accelerated T cell movement under flow as well as missing links in the track crossing points. Both are characterized by large displacement lengths such that they were not detected during the linking step, thus we will refer to both of them as “jumps” in this section. We have also eliminated short and thus unreliable segments, as well as segments which multiplicity was found to be $M = 0$ (Figure 3F). Afterward, we separated the segments into two categories, namely segments with multiplicity $M = 1$, i.e., tracks of isolated T cells, and segments with multiplicity $M > 1$ i.e. tracks of under-segmented groups of T cells, where tracks of several T cells intersected. Finally, we extended the

tracks of isolated T cells into the intersection if the branching vertex had a multiplicity of n and was splitting in exactly n segments with multiplicity $M = 1$ (Figure 3G).

Lastly, to obtain reliable T cell tracks, we performed resolving the track intersections, i.e., identifying track segments corresponding to the same T cell before and after the under-segmented track region (Figure 3H).

Detailed information on the developed under-flow T cell tracking algorithm is given in the "T-cell tracking" section of the Supplementary Material.

III. T-cell migration analysis

Next, we performed the T-cell migration analysis based on the reconstructed T cell tracks. We selected tracks which were inside the fiducial area of the FoV, namely coordinates of the T cell at all timepoints along the track were located at least 25 µm away from the bounding box enclosing all segmented T cells. Next, tracks of T cells that were touching another T cell at the end of the assay acquisition were excluded, since T cells directly adjacent to each other can hide the start of T cell transmigration across the pMBMEC monolayer and thus compromise correct detection and quantification of this step. Additionally, only tracks which had T cells assigned in at least 6 timeframes during the physiological flow phase. We also require T cells to be assigned for at least 75% of timeframes along the track. Under-segmented parts of T cell tracks were not considered. Examples of selected tracks can be seen in Supplementary Video 3.

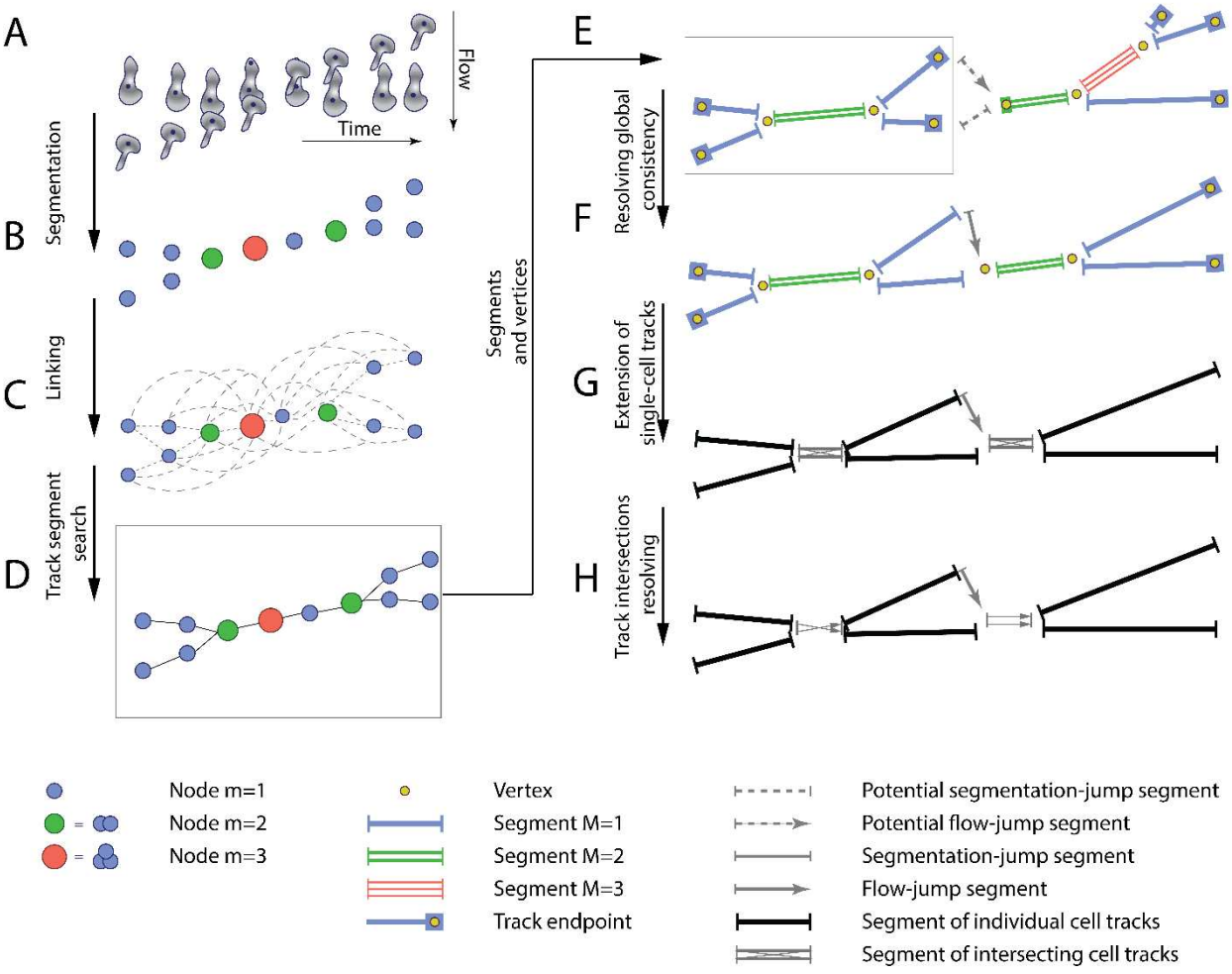

Figure 3. The T-cell tracking pipeline. A. Segmentation and centroids of two migrating T cells under flow over time. **B.** Nodes corresponding to segmented T cells. Node sizes and colors correspond denote the multiplicity estimate of a node. **C.** Nodes together with links between adjacent in space and time nodes form graph. **D.** Selected links are obtained with global optimization on the graph. **E.** Graph of segments and vertices obtained according to node multiplicity. **F.** Resolving global segment multiplicity consistency with global optimization on the graph. Additionally search for rapid displacement of segmented T cell due under-segmentation or to presence of flow is performed. **G.** Extension of tracks of individual T cells into the track intersection. **H.** Resolving track intersections.

After exclusion of the tracks of the cellular debris which were misclassified as T cells during segmentation step using a dedicated “not-a-T-cell” classifier, we performed identification of

transmigration (Supplementary Figure 5), probing and crawling migration regimes, as well as accelerated movement along the T cell track. Detailed information on the analysis of the T cell tracks is given in the "T-cell migration analysis" section of the Supplementary Material.

Finally, for each track we evaluated motility parameters for each of the following migration regimes: probing before the transmigration, crawling before the transmigration, all crawling above pMBMECs monolayer including T cell crawling segments after first transmigration attempts, all crawling below pMBMECs monolayer, whole T-cell track excluding accelerated movement and tracking inefficiency regions, as well as whole T-cell track. Specifically, we evaluated the following T-cell motility parameters: duration of each migration regime, the total vector and absolute displacements, the migration path length, the average migration speed (displacement over time), average crawling speed (path length over time), and finally the mean and standard deviation of the instantaneous speed. For the accelerated movement regime, we evaluated migration time, displacement, and average speed.

IV. Analysis of trafficking datasets

Having developed a full pipeline based on the UFMTrack framework for automated analysis of the multi-step T-cell migration cascade across the BBB model, we next aimed to compare results of automated analysis with previous studies, assess the capacity of the framework to gain novel insight into T-cell migration under flow, and evaluate its performance as compared to manual analysis.

1. CD4⁺ T cell analysis

To this end we first analyzed a total of 18 imaging datasets dedicated to understanding the multi-step migration of $CD4^+$ T cells across non-stimulated (n= 6), TNF stimulated (n=5) and IL1-β-stimulated (n=7) pMBMEC monolayers under physiological flow with the developed pipeline.

In these *in vitro* live cell imaging datasets, the phase-contrast imaging was performed as described in the "Data acquisition" section above. The T-cell accumulation phase corresponding to the shear stress of 0.1 dynes/cm^2 lasted for 32 timeframes (5min) followed by conditions of physiological flow (shear stress 1.5 dynes/cm^2) for the subsequent 160 timeframes (27min). After increasing to physiological flow rates(10), a significant number of T cells detached from the pMBMEC monolayers, with higher numbers of T cell detaching from non-stimulated pMBMEC monolayers when compared to those stimulated with pro-inflammatory cytokines as detected by the distribution of the track ending times between 5 and 30 min. (Figure 4A).

Analyzing these datasets with the established UFMTrack framework the type of T-cell behavior for each of the detected T-cell tracks and the aggregated T-cell behavior statistic was obtained for the non-stimulated and stimulated pMBMEC monolayers (Figure 4B). The data obtained with UFMTrack were found to be in accordance to our previous observations obtained by manual frame-by-frame analysis (10,12,19). We further obtained the data for T-cell migration speed, T-cell displacement and T-cell path lengths for the crawling T cells, as these are the primary cell motility parameters. As shown in Figure 4C-H, we observed statistically significant differences in the mean T-cell motility parameters depending on the pMBMECs stimulation condition. Furthermore, we observed differences in the shape of the distribution of T-cell crawling speeds which is consistent with our previous reports of underlying differences in the mechanisms mediating T-cell crawling on non-stimulated versus cytokine stimulated pMBMECs (19). While not statistically significant, we noted a trend towards an increased variance of the T cell instantaneous speed on stimulated compared to non-stimulated pMBMECs (Figure 4G). This suggests that T-cell crawling is often interrupted by T-cell recognizing specific cues on the stimulated endothelium. The T cell meandering index (MI) distribution was high on non-stimulated and lower on stimulated pMBMECs (Figure 4H) underscoring that cytokine stimulation enhances directed T-cell movement on the pMBMEC monolayer.

Since the analysis was performed automatically with UFMTrack, it allowed for deeper insights into the T-cell migration behavior on the pMBMEC monolayers than obtained by manual frame-by-frame analysis. Specifically, the detection of accelerated movement by UFMTrack enables the researcher to quantify the kinetics of individual T-cell detachment from the endothelium rather than simply quantifying a bulk T-cell detachment rate. These kinetics of detachment are reflected in the average speed experienced during accelerated movement, which is significantly lower for the IL1-b condition (Figure 4I) suggesting the need to break more bonds with the endothelium when pro-inflammatory cytokines are present.

As our UFMTrack workflow achieves sufficient segmentation efficiency to detect T cells below the pMBMEC monolayer as well as T-cell transmigration across the pMBMEC monolayer it also enables investigation of T-cell movement after the transmigration step. In Figure 4J we show the distribution of the migration speed for the transmigrated $CD4^+$ T cells. Interestingly, cytokine stimulation of pMBMECs although applied from the luminal side also affected T-cell movement at the abluminal side of the pMBMEC monolayer. While in the microfluidic device used in the present study the migration of T cells below the pMBMEC monolayer may not be biologically relevant, this analysis option will be valuable for future studies involving multilayer *in vitro* BBB models including the vascular basement membrane in addition to pericytes and astrocytes to mimic the entire neurovascular unit (7,20).

Importantly, our UFMTrack automatically detects and characterizes unusual events, such as reverse T-cell transmigration, that are easily overlooked with manual counting. We do not present the statistics here, as only a few such events were observed. When applied to the multilayer BBBs in forthcoming *in vitro* models however, systematic detection and analysis of these rare events will be important to understand T-cell migration in immune surveillance.

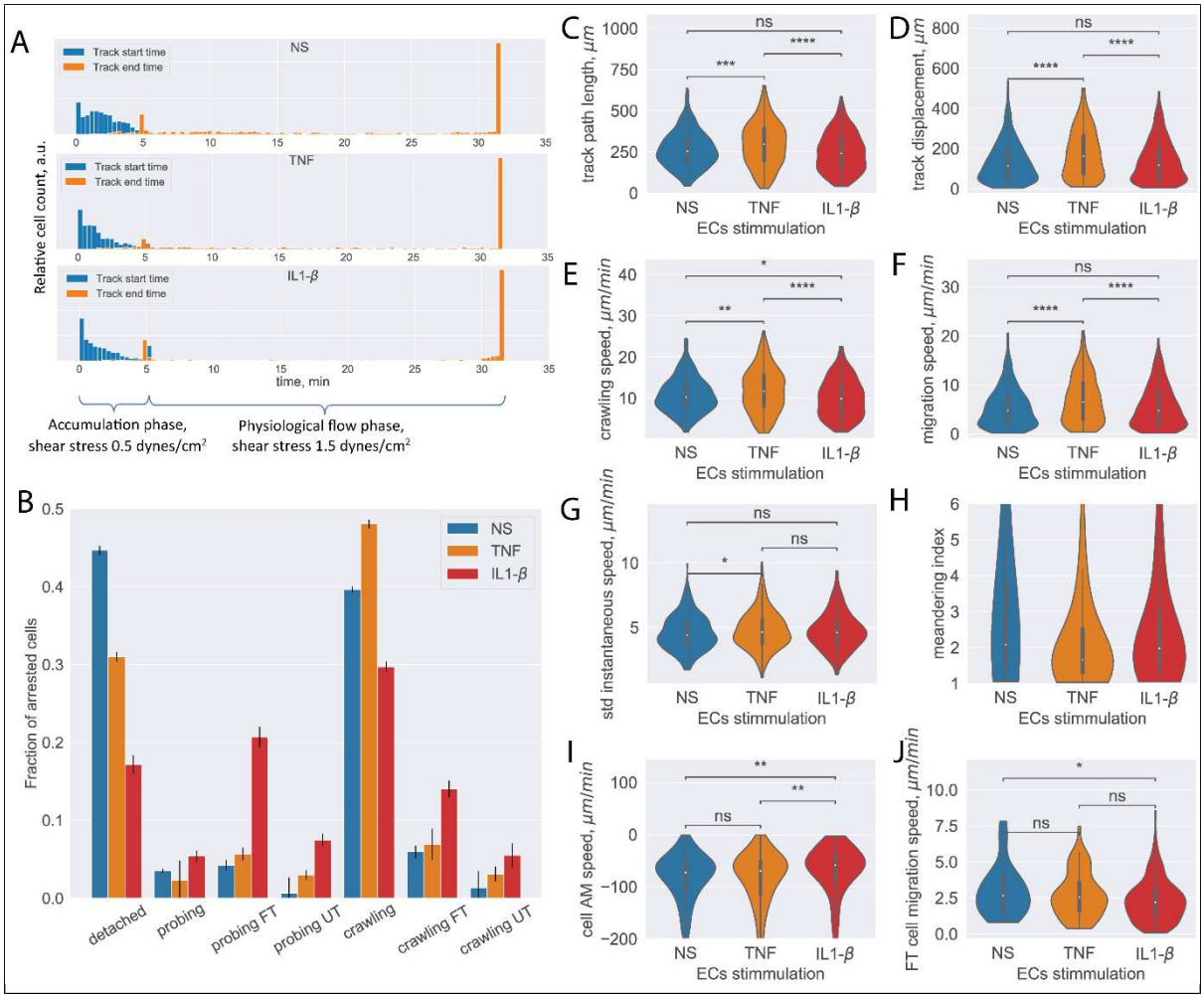

Figure 4. Analysis of CD4⁺ T-cell tracks. A. Start and end time distribution of CD4⁺ T-cell tracks on non-stimulated or TNF or IL-1β stimulated pMBMECs. More T cells detach from the non-stimulated pMBMECs after 5 minutes, when the flow is increased to physiological levels. **B.** Quantification of CD4⁺ T-cell behavior in the respective categories obtained on non-stimulated and TNF and IL-1β stimulated pMBMECs. Error bars show statistical error of the mean. (see text for details). **C-H.** Motility parameters of the crawling CD4⁺ T cells obtained for the three endothelial stimulatory conditions. Distributions of T-cell path length (**C**), displacement (**D**), crawling speed (path/time) (**E**), migration speed (displacement/time) (**F**), variability of instantaneous T-cell crawling speed along the track (standard deviation, **G**), and meandering index (**H**). **I.** Distribution of CD4⁺ T-cell accelerated movement (AM) speed is a proxy metric for the T-cell adhesion to the healthy or inflamed endothelium. **J.** Migration speed distribution of the

transmigrated CD4⁺ T cells. Stimulation applied to the luminal side of pMBMECs affects T-cell migration at the abluminal side of pMBMECs after their transmigration.

FT - T cells performed full transmigration, UT – T cells performed uncompleted transmigration.

2. CD8⁺ T cells analysis

As we have previously shown that the multi-step T-cell extravasation across pMBMEC monolayers differs between CD4⁺ and CD8⁺ T cells, we next analyzed 2 datasets studying the multi-step migration of CD8⁺ T cells across non-stimulated (NS) and TNF/ interferon-gamma (TNF/IFN-γ) stimulated pMBMEC monolayers under physiological flow over 161 timeframes (27 min). The CD8⁺ T cells were slightly different in size and appearance when compared to the CD4⁺ T cells used for training of the segmentation model. To benchmark our established UFMTrack pipeline in this more difficult configuration, the datasets were first manually analyzed by 4 experimenters: one advanced experimenter with 4 years of experience (AdEx) and three unexperienced experimenters who received comparable 2-hour introduction and training (Ex1-Ex3). The analyses were performed on the subset of the acquisition, 161 timeframes long starting from timeframe 31.

Manual cell analysis and tracking was as described in the “Materials and Methods” section separately for each of the 8 tiles of the tiled acquisition. Next all crawling CD8⁺ T cells which did not perform any transmigration were manually tracked for the timespan after the flow was increased to the physiological level using the manual tracking in ImageJ.

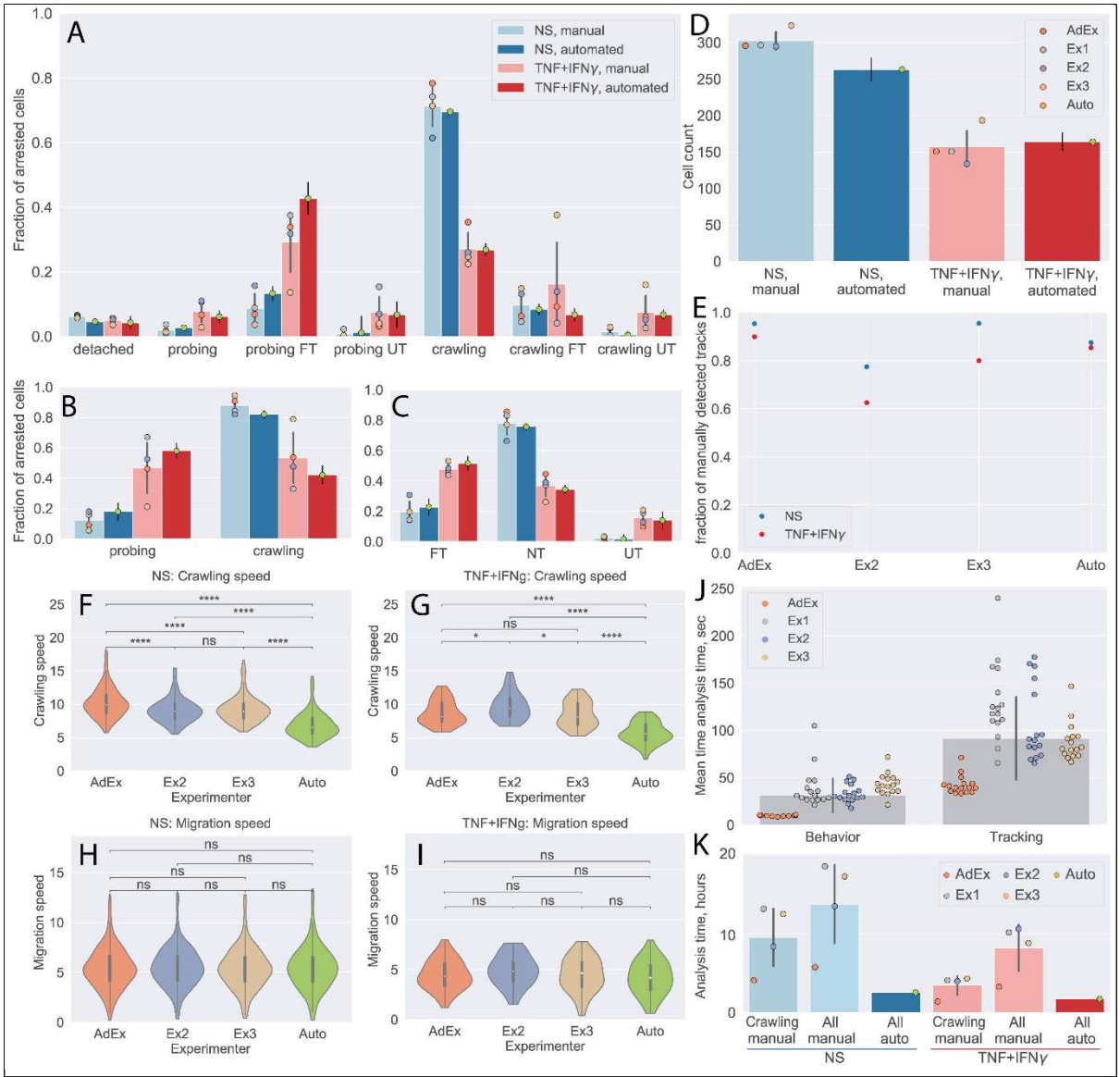

Figure 5. Comparison of automated analysis with UFMTrack and manual analysis of the CD8⁺ T-cell tracks. A-C: CD8⁺ T-cell behavior statistic obtained for non-stimulated (NS) and cytokine stimulated pMBMECs as obtained manually by four experimenters, as well as automatically with UFMTrack. **A.** Quantification of CD8⁺ T-cell behavior in the respective categories obtained on non-stimulated and TNF/IFN-γ stimulated pMBMECs is consistent with results obtained by manual frame-by-frame analysis. Cytokine stimulation of pMBMECs increases T-cell probing behavior (**B**) as well as T-cell transmigration rate (**C**). Error bars show standard deviation of the manual analysis, and statistical error of the mean for automated analysis. Points correspond to individual experimenters. **D.** Counts of CD8⁺ T cells obtained manually by four experimenters as well as

automatically by UFMTrack. The T-cell detection efficiency is above 90%. Error bars show standard deviation of the manual analysis, and statistical error of the mean for the automated analysis. Points correspond to individual experimenters. **E.** Detection efficiency of crawling CD8⁺ T cell tracks between the manual and automated analysis. **F-I.** Comparison of CD8⁺ T-cell crawling speed (path/time) (**F, G**) and migration speed (displacement/time) (**H, I**) on non-stimulated (**F, H**) and cytokine stimulated (**G, I**) pMBMECs. The T-cell position assignment error in manual tracking leads to biased crawling speed estimation. **J.** Comparison of the analysis time (per cell) required for behavior analysis and tracking of CD8⁺ T cells. **K.** Total analysis time (per dataset) for behavior analysis and tracking of CD8⁺ T cells. Comparison shown for manual analysis with tracking of crawling cells only (Crawling manual), time estimate for manual analysis with tracking of all cells (All manual), and the in-depth automated analysis of all cell tracks with UFMTrack (All auto).
FT - T cells performed full transmigration, UT – T cells performed uncompleted transmigration, NT - T cells did not perform transmigration.

First, we compared the CD8⁺ T cell behavior statistics obtained manually and by our automated analysis pipeline (Figure 5A-C). The results obtained by automated analysis were in full agreement with the manual analysis performed by the experienced experimenter. At the same time the data highlight the variability of the results from the unexperienced experimenters, confirming the potential for significant experimenter bias.

We also show detection efficiency of T cells by the UFMTrack. To achieve this goal we combined the numbers of CD8⁺ T cells detected in each tile by manual analysis. Due to the overlap between the individual tiles, some CD8⁺ T cells are seen more than once. To obtain an estimate of the total CD8⁺ T cell count detected manually, we scaled the number of CD8⁺ T cells accordingly to the number of detected unique T-cell tracks (see below). By this approach we found T-cell detection efficiency to be above 90% (Figure 5D). Lower efficiency in the NS condition can be explained by the increased T-cell density. These findings set the appropriate T-cell density for automated analysis of their migration

353 behavior on pMBMEC monolayers to 200-300 cells per FoV of the size of 3.8 mm^2, or 50-80
354 cells/mm^2.

355 Next, we compared the T-cells tracks as obtained manually by three experimenters as well as
356 automatically by our UFMTrack. To this end we first matched the tracks in adjacent tiles to obtain
357 the tracks on the whole imaging area avoiding multiple counts of the same track. This was achieved
358 by pattern matching with initial offsets between tiles obtained by an automatic frame alignment
359 procedure which was performed as part of the automatic analysis. We considered T-cell tracks
360 observed in different tiles to be tracks of the same T cell if $f_{in} > \frac{1}{2} f_{out} - 0.8$, where f_{in} is the fraction
361 of timepoints along a track at which the distance between the T cells was below 17 µm and f_{out} was
362 the fraction of timepoints along a track at which distance between cells was above 25 µm. We used
363 the same approach to match the T-cell tracks obtained by each experimenter, as well as with the
364 automated UFMTrack. To compare performance in an objective manner, we excluded manually
365 obtained tracks which lay outside of the fiducial volume of the automated analysis, as well as T cells
366 that were touching another T cell in the end of the acquisition as those were also excluded from the
367 automated analysis. We then took as 100% the sum of all T-cell tracks detected manually and
368 evaluated the fraction of the T-cell tracks detected by each experimenter as well as automatically by
369 our UFMTrack.

370 In Figure 5E, we show that our pipeline achieves a comparable T-cell tracking efficiency when
371 compared to the manual analysis. While its performance was not superior to that of the
372 experimenter with 4 years of expertise in analysis of the under-flow datasets, it does perform better
373 than less experienced experimenters.

374 We also compared the T-cell motility parameters obtained manually and automatically for the
375 non-stimulated and stimulated pMBMECs (Figure 5F-I). Data obtained for the CD8$^+$ T-cell migration
376 speed on pMBMECs was comparable between all experimenters and the automated analysis. In
377 contrast, results obtained for the T-cell crawling speed were significantly different between the

automated approach and manual analysis. Taking a closer look at the T-cell tracks (Supplementary Figure 6) we readily observed that the manual analysis contains significant errors in the assignment of the T-cell position. This leads to a jittery pattern in the T-cell migration tracks, and overestimation of T-cell path and thus T-cell crawling speed. Employing our novel automated analysis pipeline eliminated this systematic error in the measurements.

To finally investigate the potential benefit in the time required for automated versus manual data analysis we investigated the time required for a given experimenter to analyze such datasets manually using the Clockify time tracker (21). In Figure 5J we show the average time spent for performing a full T-cell behavior analysis and T-cell tracking in each imaging tile, as well as on average. Clearly the experienced experimenter outperforms the inexperienced experimenters by a factor of 3. On average a researcher would thus spend 8.1 hours for analyzing a dataset with 300 T cells when only the tracks of crawling T cells (50%, i.e. 150 cells) are analyzed. If all T-cell tracks were to be analyzed this time would further increase to 12.9 hours. Given the fact that on average 10 datasets can be produced per day, manual analysis becomes a bottleneck, leading to delays in exhaustive data analysis and thus ultimately in research progress. The UFMTrack framework enables analysis time reduction by a factor of 3 when analyzing only crawling cells and by a factor of 5 if all cell tracks are to be analyzed (Figure 5K). With average analysis time of 2.3 hours, the 10 experiments carried out in one day can be fully analyzed within one day of machine-time. This enables scalability of flow-based immune cell migration experiments, while simultaneously lifting from the researchers the burden of tedious and time-consuming manual analysis.

Discussion

In this study, we have developed the under-flow migration tracker (UFMTrack) framework. It consists of independent modules and allows for segmentation, tracking, and motility analysis of T cells, migrating on, across, and below the monolayer of primary mouse brain microvascular

403 endothelial cells under physiological flow *in vitro*. The developed method relies exclusively on phase-
404 contrast imaging data. Therefore, it does not require to establish fluorescent labels of the migrating
405 immune cell population to be studied, avoids potential photo-toxicity to be considered for
406 fluorescent imaging modalities (22–24), and is thus the preferred choice for analyzing trafficking of
407 sensitive cell types. T-cell segmentation and prediction of the transmigrated T cell areas is
408 performed using custom 2D+T U-Net like convolutional neural network. It enables reliable
409 segmentation of T cells both above and below the pMBMEC monolayer. The existing particle and cell
410 tracking toolkits consider migration of one cell type, thus are not suitable for detection of distinct
411 migration regimes and cell interactions (25–28). Furthermore, to the best of our knowledge none of
412 the existing algorithms consider migration under flow causing rapid cell displacement. The tracking
413 of T cells interaction with the pMBMECs during all migration regimes under physiological flow
414 required designing of a new tracking algorithm considering rapid T-cell appearance, disappearance,
415 and displacement in the field of view caused by the flow. We have also developed approaches that
416 resolve track intersections, i.e. identifying track segments corresponding to the same T cell before
417 and after under-segmented track regions, which are inevitable during T-cell migration. By
418 establishing the detection of T-cell crawling, probing, transmigration, and accelerated movement
419 combined with reliable T-cell tracking, we have enabled the in-depth analysis of distinct migration
420 regimes on a cell-by-cell basis. By reducing the dataset analysis time by a factor of 5, UFMTrack
421 allows for performing a thorough analysis of 10 experiments that can be carried out by a researcher
422 in one day within one day of machine-time. We have demonstrated that the automated analysis
423 performs on par with manual analysis while improving accuracy and eliminating experimenter bias,
424 and enables scalability of flow-based immune cell migration experiments by and reducing the
425 analysis cost and lifting the burden of time-consuming manual analysis.

426 In this work we have demonstrated the applicability of the developed framework to the analysis
427 of the multi-step extravasation of $CD4^+$ and $CD8^+$ T cells across non-stimulated or cytokine
428 stimulated pMBMEC monolayers under physiological flow. We have also demonstrated that the

developed framework allows for automated analysis of T-cell behavior statistics, and motility parameters of distinct T-cell migration regimes. Results of the automated analysis of $CD4^+$ T-cell behavioral statistics performed with UFMTrack are in agreement with previous studies using manual data analysis (12). The automated analysis of datasets of $CD8^+$ T-cell migration has shown comparable performance with manual analysis performed by one experimenter with 4 years of analysis experience and three less experienced experimenters. At the same time the variance of the results obtained manually showed significant experimenter bias that the automated analysis eliminated. Additionally, automated analysis allowed for in depth analysis of all T-cell migration categories and precise evaluation of T-cell motility parameters, which was not achieved by manual T-cell tracking, even by the most experienced user.

Quantification of the fraction of transmigrated T cells is crucial for studying the molecular mechanisms governing infiltration of autoaggressive T cells across the BBB into the CNS parenchyma and the immune surveillance. The role of specific endothelial or T-cell adhesion molecules in influencing the dynamic interactions of T cells with pMBMECs can e.g. be probed by quantifying the ratio of T-cell crawling behavior to T-cell probing. With the analysis procedure established in the UFMTrack framework the number of times a T cell interrupts its crawling regime switching to short probing behavior on the endothelium can be evaluated, thus providing information on the distribution of “hot-spots” on the endothelium. Additionally, experiment scalability and the analysis on a cell-by-cell basis enables the search for distinct populations of T-cells, e.g., according to the distribution of probing to crawling behavioral ratios. The strength of T-cell adhesion to the endothelium can be probed with the developed framework using the measure of T-cell detachment rate, and the distribution of the previously overlooked T cell accelerated movement occurrences and accelerated movement speed. Finally, the possibility of quantifying the motility parameters of the transmigrated T cells enables future studies involving multilayer *in vitro* BBB models including the vascular basement membrane in addition to mural cells such as pericytes and astrocytes mimicking the entire neurovascular unit.

While in this work we have focused on the analysis of mouse T cells interacting with pMBMEC under flow, the methods we present establish a foundation for a broad range of studies involving *in vitro* under-flow studies of immune cell trafficking. The tracking algorithm and motility analysis developed in the UFMTrack framework is also directly applicable for the analysis of immune cells interaction with recombinant protein under flow, employing either pure phase-contrast imaging or epi-fluorescent imaging when studying fluorescently labeled immune cells. The T-cell segmentation based on deep neural networks can be applied to studies of trafficking of other immune cell subsets on and across the pMBMEC monolayer. The application to immune cell trafficking across other endothelial monolayers including those from different species or vascular beds as well as lymphatic endothelial cells is possible but requires fine-tuning of the trained segmentation model. While training of the models presented here required a large dataset of annotated T-cell masks, and transmigration masks, this can be largely avoided for future development. Future models can be developed more efficiently by leveraging our existing annotated dataset of T-cell migration on the pMBMECs while employing transfer learning approaches in a multitask framework with weak supervision and fluorescent labels as auxiliary learning targets to adapt the model for segmentation of cells with different appearances. This can be further improved by adopting self-supervised contrastive learning methods which have demonstrated significant advancements for model pretraining in recent years. This is the subject of our future studies. By sharing the data and open-source code of the UFMTrack framework, i.e. the training data used for the segmentation model training, trained models, as well as the model architecture, and full under-flow T-cell tracking and migration analysis pipeline, we hope to encourage the community to pursue these developments to advance the field.

One current limitation of the method is the performance reduction of the T-cell tracking when the density of migrating T cells significantly increases (>250 cells/dataset). Thus the recommended T cell concentration is about 100-150k/ml. However to avoid non-physiological interactions between migrating T cells, as well as T cell clumping, the T-cell density should be kept at moderate levels

anyway. Additionally, by analyzing data from 8 stitched fields of view allows obtaining comparable statistics. The current analysis of the behavioral statistics quantifies the fraction of different T-cell migration regimes with respect to the number of the adhered cells instead of the total T-cell count passing through the microfluidic device. While the number of fast-moving T cells during the accumulation phase cannot be directly counted using the imaging modality employed here, it can be potentially estimated indirectly from the imaging data with additional calibration experiments and a dedicated machine learning model. Another limitation is that currently we do not consider dividing immune cells. While cell division events happen rarely (<1% of T cells) and are not of primary events for the study of immune cell interaction with the BBB model, the modular architecture of our framework will facilitate future extension to detect cell division.

By enabling experiment scalability, unbiased analysis with advanced accuracy and an in-depth analysis of large datasets of T-cell dynamics under flow, the computational and analytical framework presented here contributes to the 3R principle when studying the interaction of cells derived from animal models by reducing the number of animals to be sacrificed. UFMTrack can be employed for fundamental research of the molecular mechanisms governing immune cell trafficking across a range of vascular beds, screening of pharmaceutical treatments, as well as for personalized medicine based on evaluation of treatment efficacy on patient derived T-cell migration behavior on patient derived endothelial monolayers. Eventually, the developed framework can be extended to real-time operation during image acquisition. Combined with transgenic photo-convertible immune cells allowing for photoconversion of immune cells according to their behavior will allow for subsequent fluorescent cell sorting and scRNA-Seq analysis. Such advanced studies are needed to reveal the role of genetic differences governing T-cell migration regimes.

Materials and Methods

1. *pMBMEC cell culture*

Primary mouse brain microvascular endothelial cells (pMBMECs) were isolated from 8-12 weeks old C57BL/6J WT mice and cultured exactly as described before (10,29). Intact monolayers were stimulated or not with 10 ng/mL of recombinant mouse TNF, 20 ng/mL of recombinant mouse IL1-β for, or 5ng/mL recombinant mouse TNF + 100 U/mL recombinant mouse IFN-γ 16-24 hours prior to the assays as previously described (19).

2. *T cell preparation*

Naïve $CD4^+$ and $CD8^+$ T-cell isolation: Peripheral lymph nodes and spleens from 2D2 and OT-I C57BL/6J mice were harvested and single cell suspensions were obtained by homogenization and filtration through a sterile 100 μm nylon mesh. A second filtration was applied after erythrocyte lysis (0.83% NH_4Cl, Tris-HCl). 2D2 and OT-I cells were isolated respectively with magnetic $CD4^+$ and $CD8^+$ T cell selection beads (EasySep, STEMCELL Technologies).

In vitro activation of naïve $CD8^+$ T cells: OT-I $CD8^+$ T cells were activated as described before (29,30). Activated $CD8^+$ T cells were cultured in IL-2 containing media for 3 days post-activation.

In vitro activation of naïve $CD4^+$ T cells: 2D2 $CD4^+$ T cells were activated as described before (19). Activated $CD4^+$ T cells were cultured in IL-2 containing media for 24 additional hours.

3. *In vitro under-flow T-cell migration assay*

We studied the multi-step T-cell migration across monolayers of primary mouse brain microvascular endothelial cells (pMBMECs) in a microfluidic device under physiological flow by *in vitro* live-cell imaging according to the previously established procedure (12,19). pMBMECs that

were previously cultured in Ibidi µ-Dish to confluency and a custom-made flow chamber was placed on top of the pMBMECs culture and connected to the flow system filled with migration assay medium (MAM) (10). During the accumulation phase, T cells at concentration between 55k/ml and 166k/ml were superfused for 5 minutes under low shear stress of 0.1 dynes/cm^2 allowing them to settle on top of the pMBMEC monolayer. We used lower T cell concentration as compared to previous studies to enable automated T-cell interaction analysis. Afterwards, the flow was increased to physiological levels with a flow shear stress of 1.5 dynes/cm^2 to study post-arrest T-cell behavior on pMBMECs for 27 minutes (Figure 1A, B).

4. Data acquisition

The timelapse imaging was performed during both accumulation and physiological flow phases using phase-contrast imaging at a framerate of 6 frames/min, and resolution of 0.629um/pixel. In this modality the acquired images are gray scale, and the T cells, especially after the migration across the pMBMEC monolayer, have a similar appearance to the pMBMECs, making the T-cell segmentation task very challenging (Figure 1C). The data was acquired in tiles of 870 × 650 µm^2 (1389 × 1041 pixels) with an overlap of 100 µm, leading to a total acquired image area of 3170 × 1220 µm^2. For each experiment the dataset consists of 30 timeframes of T-cell accumulation and 162 timeframes of dynamic T-cell interactions with the pMBMEC monolayer under physiological flow. The timestep between sequential timeframes for each tile is 10 s. The total acquired area is thus limited by the acquisition speed, or by the flow chamber size.

5. Manual analysis of T-cell migration

Manual cell analysis and tracking was performed according to previously established procedure using ImageJ software (ImageJ software, National Institute of Health, Bethesda, MD, USA) (11). The number of arrested T cells was thus counted at timeframe 33 of the subset. The behavior of arrested T cells was defined and expressed as fractions of arrested T cells set to 100% as follows:

- T cells that detached during the observation time ("detached")
- T cells that migrated out of the FoV detached during the observation time ("out of FoV")
- T cells that continuously crawled on the pMBMEC monolayer ("crawling")
- T cells that remained in the same location (displacement less than twice the cell size) while actively interacting with pMBMEC monolayer ("probing")
- T cells that crossed the pMBMEC monolayer with or without prior crawling ("crawling full transmigration" and "probing full transmigration"). The event of T-cell transmigration across the pMBMECs monolayer became obvious due to the change of appearance of the transmigrated part of the T cells from phase bright (on top of the pMBMECs monolayer) to phase dark.
- T cells that partially crossed the pMBMEC monolayer, then retracted the protrusions and continued to migrate above the monolayer ("crawling uncompleted transmigration" and "probing uncompleted transmigration").

6. UFMTrack performance evaluation

The inference of T cell masks and transmigration masks was performed on a dual-CPU Intel(R) Xeon(R) CPU E5-2670 v3 @ 2.30GHz, 256GB RAM node equipped with 8 Graphical Processing Units (GPU) NVIDIA GeForce GTX TITAN X / GeForce GTX 1080. Frame alignment and segmentation were performed on an Intel(R) Core(TM) CPU i7-4771 @ 3.50GHz, 32GB RAM workstation with NVIDIA GeForce GTX TITAN GPU. Cell tracking was performed on a dual-CPU Intel(R) Xeon(R) CPU E5-2643 v2 @ 3.50GHz, 256GB RAM workstation.

Acknowledgements

We owe sincere thanks to Dr. James McGrath and Danial Ahmad (Rochester University , NY, USA) for their detailed and insightful feed-back to our manuscript. This work was supported by an

UniBe ID Grant to MV, BE and AA and the Microscopy Imaging Center (MIC) of the University of Bern.

Data Availability

The source code for the T-cell segmentation models, data preprocessing, training, performance evaluation, and inference scripts are available on GitHub at https://github.com/neworldemancer/UFMSegm. This repository also contains win64 binaries used for the watershed-based segmentation of the predicted T cell probability maps and transmigration probability maps.

The source code for the under-flow T-cell tracking and T-cell migration analysis, along with the scripts used for performance evaluation of the framework is available on GitHub at https://github.com/neworldemancer/UFMTrack.

The training phase-contrast data with manual annotations, the reference datasets for histogram normalization, as well as trained models are available on Zenodo: [http://doi.org/10.5281/zenodo.7489557].

The datasets used for evaluation of our framework are available on Zenodo: [http://doi.org/10.5281/zenodo.7489972, http://doi.org/10.5281/zenodo.7489984, http://doi.org/10.5281/zenodo.7489996, http://doi.org/10.5281/zenodo.7490012, http://doi.org/10.5281/zenodo.7490020, http://doi.org/10.5281/zenodo.7490029].

References

1. Marchetti L, Engelhardt B. Immune cell trafficking across the blood-brain barrier in the absence and presence of neuroinflammation. Vasc Biol [Internet]. 2020 Apr 10 [cited 2022

Oct 28];2(1):H1–18. Available from: https://vb.bioscientifica.com/view/journals/vb/2/1/VB-19-0033.xml

2. Nishihara H, Soldati S, Mossu A, Rosito M, Rudolph H, Muller WA, et al. Human CD4+ T cell subsets differ in their abilities to cross endothelial and epithelial brain barriers in vitro. Fluids Barriers CNS [Internet]. 2020 Feb 3 [cited 2022 Apr 14];17(1):1–18. Available from: https://fluidsbarrierscns.biomedcentral.com/articles/10.1186/s12987-019-0165-2

3. Nourshargh S, Alon R. Leukocyte Migration into Inflamed Tissues. Immunity. 2014 Nov 20;41(5):694–707.

4. Nourshargh S, Hordijk PL, Sixt M. Breaching multiple barriers: leukocyte motility through venular walls and the interstitium. Nat Rev Mol Cell Biol 2010 115 [Internet]. 2010 May [cited 2022 Dec 23];11(5):366–78. Available from: https://www.nature.com/articles/nrm2889

5. Bartholomäus I, Kawakami N, Odoardi F, Schläger C, Miljkovic D, Ellwart JW, et al. Effector T cell interactions with meningeal vascular structures in nascent autoimmune CNS lesions. Nat 2009 4627269 [Internet]. 2009 Oct 14 [cited 2022 Oct 28];462(7269):94–8. Available from: https://www.nature.com/articles/nature08478

6. Lyck R, Engelhardt B. Going Against the Tide – How Encephalitogenic T Cells Breach the Blood-Brain Barrier. J Vasc Res [Internet]. 2012 Oct [cited 2020 Mar 10];49(6):497–509. Available from: https://www.karger.com/Article/FullText/341232

7. Dias MC, Quesada AO, Soldati S, Bösch F, Gruber I, Hildbrand T, et al. Brain endothelial tricellular junctions as novel sites for T cell diapedesis across the blood-brain barrier. J Cell Sci [Internet]. 2021 Apr 1 [cited 2022 Oct 28];134(8). Available from: https://pubmed.ncbi.nlm.nih.gov/33912914/

8. Steinman L, Zamvil SS. Virtues and pitfalls of EAE for the development of therapies for multiple sclerosis. Trends Immunol [Internet]. 2005 [cited 2022 Dec 23];26(11):565–71.

Available from: https://pubmed.ncbi.nlm.nih.gov/16153891/

9. Singer BA. The role of natalizumab in the treatment of multiple sclerosis: benefits and risks. Ther Adv Neurol Disord [Internet]. 2017 Sep 1 [cited 2022 Dec 23];10(9):327–36. Available from: https://pubmed.ncbi.nlm.nih.gov/28861122/

10. Steiner O, Coisne C, Cecchelli R, Boscacci R, Deutsch U, Engelhardt B, et al. Differential Roles for Endothelial ICAM-1, ICAM-2, and VCAM-1 in Shear-Resistant T Cell Arrest, Polarization, and Directed Crawling on Blood–Brain Barrier Endothelium. J Immunol [Internet]. 2010 Oct 15 [cited 2022 Oct 23];185(8):4846–55. Available from: https://www.jimmunol.org/content/185/8/4846

11. Rudolph H, Klopstein A, Gruber I, Blatti C, Lyck R, Engelhardt B. Postarrest stalling rather than crawling favors CD8 $^{+}$ over CD4 $^{+}$ T-cell migration across the blood-brain barrier under flow in vitro. Eur J Immunol [Internet]. 2016 Sep 1 [cited 2019 Apr 19];46(9):2187–203. Available from: http://doi.wiley.com/10.1002/eji.201546251

12. Abadier M, Jahromi NH, Alves LC, Boscacci R, Vestweber D, Barnum S, et al. Cell surface levels of endothelial ICAM-1 influence the transcellular or paracellular T-cell diapedesis across the blood–brain barrier. 2015 Apr 1 [cited 2019 Apr 19];45(4):1043–58. Available from: http://doi.wiley.com/10.1002/eji.201445125

13. Shulman Z, Shinder V, Klein E, Grabovsky V, Yeger O, Geron E, et al. Lymphocyte Crawling and Transendothelial Migration Require Chemokine Triggering of High-Affinity LFA-1 Integrin. Immunity. 2009 Mar 20;30(3):384–96.

14. Arts JJG, Mahlandt EK, Grönloh MLB, Schimmel L, Noordstra I, Gordon E, et al. Endothelial junctional membrane protrusions serve as hotspots for neutrophil transmigration. Elife. 2021 Aug 1;10.

15. Ronneberger O, Fischer P, Brox T. U-Net: Convolutional Networks for Biomedical Image

Segmentation. 2015 May 18 [cited 2017 Oct 25]; Available from: http://arxiv.org/abs/1505.04597

16. Abadi M, Barham P, Chen J, Chen Z, Davis A, Dean J, et al. TensorFlow: A system for large-scale machine learning. [cited 2022 Oct 23]; Available from: https://tensorflow.org.

17. Schiegg M, Hanslovsky P, Kausler BX, Hufnagel L, Hamprecht FA. Conservation Tracking. 2013;

18. Perron L, Furnon V. OR-Tools [Internet]. Available from: https://developers.google.com/optimization/

19. Haghayegh Jahromi N, Marchetti L, Moalli F, Duc D, Basso C, Tardent H, et al. Intercellular Adhesion Molecule-1 (ICAM-1) and ICAM-2 Differentially Contribute to Peripheral Activation and CNS Entry of Autoaggressive Th1 and Th17 Cells in Experimental Autoimmune Encephalomyelitis. Front Immunol. 2020 Jan 14;10:3056.

20. Mossu A, Rosito M, Khire T, Li Chung H, Nishihara H, Gruber I, et al. A silicon nanomembrane platform for the visualization of immune cell trafficking across the human blood–brain barrier under flow. J Cereb Blood Flow Metab [Internet]. 2019 Mar 1 [cited 2022 Dec 21];39(3):395–410. Available from: https://journals.sagepub.com/doi/10.1177/0271678X18820584

21. Clockify. Clockify™ - 100% FREE Time Tracking Software [Internet]. 2022 [cited 2022 Oct 23]. Available from: https://clockify.me/

22. Jae Oh D, Min Lee G, Francis K, Palsson BO. Phototoxicity of the Fluorescent Membrane Dyes PKH2 and PKH26 on the Human Hematopoietic KG1a Progenitor Cell Line. [cited 2022 Dec 23]; Available from: https://onlinelibrary.wiley.com/terms-and-conditions

23. Saetzler RK, Jallo J, Lehr HA, Philips CM, Vasthare U, Arfors KE, et al. Intravital Fluorescence Microscopy: Impact of Light-induced Phototoxicity on Adhesion of Fluorescently Labeled Leukocytes. J Histochem Cytochem. 1997;45(4):505–13.

671 24. Purschke M, Rubio N, Held KD, Redmond RW. Phototoxicity of Hoechst 33342 in time-lapse
672 fluorescence microscopy. Photochem Photobiol Sci [Internet]. 2010 [cited 2022 Dec
673 23];9(12):1634–9. Available from: https://pubmed.ncbi.nlm.nih.gov/20931137/

674 25. Allan DB, Caswell T, Keim NC, van der Wel CM, Verweij RW. Trackpy. 2021 Apr 13 [cited 2022
675 Oct 29]; Available from: https://zenodo.org/record/4682814

676 26. Tsai HF, Gajda J, Sloan TFW, Rares A, Shen AQ. Usiigaci: Instance-aware cell tracking in stain-
677 free phase contrast microscopy enabled by machine learning. SoftwareX. 2019 Jan 1;9:230–7.

678 27. Ershov D, Phan MS, Pylvänäinen JW, Rigaud SU, Le Blanc L, Charles-Orszag A, et al. TrackMate
679 7: integrating state-of-the-art segmentation algorithms into tracking pipelines. Nat Methods
680 2022 197 [Internet]. 2022 Jun 2 [cited 2022 Oct 29];19(7):829–32. Available from:
681 https://www.nature.com/articles/s41592-022-01507-1

682 28. Ulicna K, Vallardi G, Charras G, Lowe AR. Automated Deep Lineage Tree Analysis Using a
683 Bayesian Single Cell Tracking Approach. Front Comput Sci. 2021 Oct 20;3:92.

684 29. Coisne C, Lyck R, Engelhardt B. Live cell imaging techniques to study T cell trafficking across
685 the blood-brain barrier in vitro and in vivo. Fluids Barriers CNS [Internet]. 2013 Jan 21 [cited
686 2020 Mar 9];10(1):7. Available from: http://www.ncbi.nlm.nih.gov/pubmed/23336847

687 30. Rudolph H, Klopstein A, Gruber I, Blatti C, Lyck R, Engelhardt B. Postarrest stalling rather than
688 crawling favors CD8+ over CD4+ T-cell migration across the blood–brain barrier under flow in
689 vitro. Eur J Immunol [Internet]. 2016 Sep 1 [cited 2020 Mar 9];46(9):2187–203. Available
690 from: https://onlinelibrary.wiley.com/doi/full/10.1002/eji.201546251

691

692 **Supporting information captions**

693 **Supplementary Table 1**: Architecture of the 2D fully convolutional model for T-cell segmentation.

694 **Supplementary Table 2**: Architecture of the 2D+T fully convolutional model for T-cell
695 segmentation

696 **Supplementary Table 3:** Node variables used in global optimization during link search.

697 **Supplementary Figure 1. Training curves**. **A.** Learning rate attenuation along model training.

698 **B.** Loss value evolution along model training.

699 **Supplementary Figure 2. Comparison of the 2D and 2D+T cell segmentation models**
700 **performance for the T cell mask and transmigration mask prediction.** F1, Jaccard index, and AP
701 metrics are shown.

702 **Supplementary Figure 3: Parametrization of nodes connections for tracking. A.** Representation
703 of nodes for track segment search. Connection multiplicity for each link is obtained with global
704 optimization. **B.** Representation of vertices and segments for global multiplicity consistency
705 optimization. Connection multiplicity for each segment attached to a vertex is obtained with global
706 optimization.

707 **Supplementary Figure 4: Under flow tracking parametrization. A**. Negative log-likelihood w_{sj0} of
708 the potential T cell jump segments due to under-segmentation. **B-D.** Negative log-likelihood w_{fj0} of
709 the potential T cell jumps segments due to the flow. **B**: dt=1, **C**: dt=2, **D**: dt=3. **E.** Attenuation of the
710 vertex "not-connected" weight with time allows accounting for T cell accumulation phase at
711 timeframes 5 through 30 and increase of the flow to physiological level at timeframe 30. Blue curve
712 shows attenuation factor on the left side, i.e. corresponding to track start, and orange curve shows
713 attenuation factor on the right left side corresponding to the end of the track due to cell detachment
714 under flow.

715 **Supplementary Figure 5. Transmigration detection.** Based on the filtered transmigration factor
716 $t_{c,f}$ we obtained Boolean masks for partial and full transmigration. Next we obtained Boolean masks
717 for T-cell migration before transmigration, during uncompleted, direct, full, and reverse
718 transmigrations.

719 **Supplementary Figure 6. Comparison of reconstructed T cell tracks with result of manual**
720 **analysis.** Overlay of crawling $CD8^+$ T-cell crawling tracks on top of non-stimulated (top) and TNF/
721 IFN-γ stimulated pMBMECs (bottom) tracked manually by three experimenters as well as
722 automatically. Errors in manual tracking led to jittery pattern in the T-cell tracks. This lead in turn to
723 overestimation of the T cell crawling speed.

724 **Supplementary Video 1.** Phase-contrast time-lapse image sequence of CD4 T cells interacting
725 with IL-1β stimulated endothelium. 8 tiles of the imaging are aligned and stitched together.

726 **Supplementary Video 2.** Segmented T cells in phase-contrast time-lapse image sequence of CD4
727 T cells interacting with IL-1β stimulated endothelium. Mask of the segmented T cell is overlayed in
728 red. Transmigration probability map is overlayed in yellow.

729 **Supplementary Video 3.** Tracks of T cells reconstructed in phase-contrast time-lapse image
730 sequence of CD4 T cells interacting with IL-1β stimulated endothelium. Tracks after the increase of
731 the flow to shear stress level of 1.5 dynes/cm^2 are shown. Only tracks included in the analysis are
732 show. *see text for details

733

734